Journal of
Marine Science and Engineering

MDPI

Article

Numerical Simulation of the Behavior of Caisson Based on Physical Modeling

Sifen Huang [1], Yuwei Han [2], Shuyi Li [3] and Mi Zhou [3,*]

[1] Guangdong Shunde Power Design Institute Co., Ltd., Foshan 528399, China; hsf@sdepdc.com
[2] Guangzhou Airport Construction Investment Group Co., Ltd., Guangzhou 510640, China; hanyuwei_@gz.gov.cn
[3] State Key Laboratory of Subtropical Building Science, South China Institute of Geotechnical Engineering, South China University of Technology, Guangzhou 510640, China; li_shuyi1998@163.com
* Correspondence: zhoumi@scut.edu.cn

Abstract: Stiffened caissons are a new kind of offshore platform foundation which has been widely used in recent years. Stiffeners are employed to avoid buckling during the installation process. However, they also create a significant challenge in terms of understating the soil-flow patterns and corresponding installation resistance prediction. Although centrifuge and in situ tests can simulate the caisson installation process very well, their high costs prevent their widespread application. Model tests have been widely used in research on caisson behavior during installation, as they are convenient and cost less compared to centrifuge and prototype tests. However, the quantitative conclusions of the resulting predictions of installation resistance have some uncertainties because it is quite hard to strictly follow the similarity principle in 1 g model tests. Therefore, it is important to establish a method to calibrate the data from model tests, providing better estimates of caisson behavior in field tests. In our research, large deformation finite element (LDFE) analyses were conducted to provide insights into differences in the outcomes of caisson installation approaches between prototype tests and 1 g model tests. Prior to carrying out parametric studies, validations were conducted with good results. The results show that normalized soil strength significantly influences the behavior of caissons of various dimensions in 1 g model tests. In uniform clay, caissons exhibit consistent installation behavior; otherwise, they show significant differences. Based on systematic research, this paper reveals the mechanisms of the difference between model tests and prototype tests with different sizes of caissons and identifies the factors influencing these differences.

Keywords: suction stiffened caissons; LDFE; soil-flow mechanism; penetration resistance

check for updates

Citation: Huang, S.; Han, Y.; Li, S.; Zhou, M. Numerical Simulation of the Behavior of Caisson Based on Physical Modeling. *J. Mar. Sci. Eng.* **2024**, *12*, 1284. https://doi.org/10.3390/jmse12081284

Academic Editor: Dong-Sheng Jeng

Received: 6 June 2024
Revised: 22 July 2024
Accepted: 25 July 2024
Published: 31 July 2024

Copyright: © 2024 by the authors. Licensee MDPI, Basel, Switzerland. This article is an open access article distributed under the terms and conditions of the Creative Commons Attribution (CC BY) license (https://creativecommons.org/licenses/by/4.0/).

1. Introduction

A stiffened caisson is a large-diameter, thin-walled, cylindrical structure made of steel or reinforced concrete, extensively applied to deepwater projects and wind power engineering, such as breakwaters and gravity platforms. Examples include Floating Production Storage and Offloading (FPSO), Tension Leg Platforms (TLPs), and Deep-draft Pillar-Type Platforms (SPARs). These caissons are favored for their low construction cost, short construction period, suitability for deep water and soft soil, and reusability.

Study of the behavior of foundations in deep water has been carried out for more than 30 years, with numerical simulations having been adopted. Ram and Mohana [1] studied the behavior of offshore wind turbines (OWT) in dense sand using finite element analysis (FEA). Wang et al. [2] conducted both experimental and numerical studies to investigate the lateral response of pile groups for offshore wind turbines in sand. Recently, Alnmr and Mayassah [3] discussed innovations and future prospects for offshore wind turbines. Model tests are widely conducted to reveal the penetration resistance and soil-flow patterns during the penetration of structures. Conducting experiments on engineering prototypes would consume significant manpower and material resources and is often impractical due

to the prototype's large size. Therefore, model tests at 1× g are typically performed using reduced-scale models. Centrifuge tests are the most convenient method to provide artificial gravity fields, thereby reducing the model size and making it possible to simulate the normal stress level and capture behavior similar to that in prototype. However, centrifuge tests are expensive and difficult to operate. In contrast, 1× g model tests are cost-effective and convenient to conduct.

The scaling laws differ significantly between tests conducted at increased gravity levels (n× g) and those conducted at 1 g [4–7]. To accurately simulate the real performance of a structure in soil, 1× g model tests must follow similarity principles. Among these principles, the geometric similarity criterion is easy to follow. However, preparing soil materials according to the similarity principle and simulating the stress level in 1 g model tests is a significant challenge. Without following similarity principle, the results will exhibit a significant scale effect compared to that in prototype. Currently, there is no conversion mechanism between prototype and model tests, which limits the popularization and application of model tests.

Previous studies have indicated that when the failure mechanism involves the rotation failure of the bottom stiffener, the gap between the stiffeners will be filled with soil, resulting in dead angles above and below the bottom stiffener where soil becomes trapped [8]. Soil flow then occurs inside the caisson, and the soil is confined by the pipe wall, making it challenging to capture the soil flow characteristics within the pipe using centrifuge or standard model tests.

For centrifuge tests, Hossain and Lehane [9] carried out semi-model tests adopting two skirts-plates with stiffeners horizontally installed on both side of the skirts in order to study the penetration resistance and soil-flow patterns during the installation process in homogeneous clay and non-homogeneous clay. Zhou [10] studied the penetration resistance characteristics and soil flow mechanism of a stiffened caisson in uniform clay through the RITSS method. Through this method, it was confirmed that there was a large disturbance caused by the stiffeners in the internal soil around the caissons during the process of penetrating a stiffened caisson into normal consolidation soil; this affected the performance of the suction caisson and reduced the bearing capacity of the foundation. In terms of the anti-overturning performance of caissons, a series of laboratory tests (1× g and centrifuge) and numerical simulations were conducted by Faizi et al. [11] to explore the behavior of a caisson foundation under lateral loads and establish a comprehensive model. Through a series of 1× g model tests (at a 1/70 scale), centrifuge model tests (at 70× g acceleration), and finite element (FE) simulations, the performance of a new type of foundation, the winged caisson, in sandy soil was also studied by Faizi et al. [12]. Therefore, various studies on stiffened caissons have focused on soil-flow patterns during penetration and the characteristics of the soil around the structure after a disturbance, such as the study on the penetration resistance and bearing characteristics (the stability of a steel pile foundation). Therefore, it is of great significance to study the soil flow mechanism during penetration.

To ensure that the results of our scale model test accurately reflected the working performance of the prototype, the RITSS large deformation finite element method was employed in this study to investigate the differences in the penetration characteristics between the model stiffened caisson and the prototype caisson in homogeneous clay and normally consolidated soil. This study examines the similarities and differences between a model caisson and a prototype caisson under conditions where the similarity principle is both satisfied and not satisfied.

The research explores performance variations between the prototype caisson and the large-scale model caisson under various conditions, including different penetration depths, soil strengths, and stiffener sizes. By establishing the relationship between the model test results and the prototype test, it is demonstrated that model tests can effectively replace centrifuge tests and in situ tests. This approach leverages the advantages of model tests for better application in actual projects.

2. Finite Element Numerical Model

Hu and Randolph [13] presented the Remeshing and Interpolation Technique with Small Strain model (RITSS), a practical large deformation finite element (LDFE) method to solve large strain or large deformation problems in solid bodies (especially soil). Similar to the arbitrary Lagrangian-Eulerian approach, it uses a series of small strain finite element analyses to simulate a larger deformation finite element analysis, which combines infinitesimal strain analysis with coordinate updates, domain remeshing, and parameter interpolation. This technique uses a fully automatic remeshing method based on normal offsetting, Delaunay triangulation, and Laplacian smoothing, ensuring efficiency and robustness.

This study has investigated a stiffened caisson with length L and diameter D, penetrating into homogeneous clay. As shown in Figure 1, t is the wall thickness of the caisson, the height and width of the lateral stiffener are, respectively, h and b, and w is the bottom spacing between the caisson and the stiffener. The stiffener interval, s, is equal to w in this paper, while d is the penetration depth and α is the friction coefficient between the structures and clay. This study explores the soil flow patterns and installation resistance characteristics of stiffened caissons in homogeneous clay, considering both the prototype and model sizes. The caisson diameter (D) ranged from 0.04 to 4 m, while penetration depth d, the ratio of stiffener width to wall thickness b/t, the ratio of the stiffener spacing to the heigh of stiffener s/h, and friction coefficient α were based on the penetration characteristics at the prototype size and model size. Triangular elements with six nodes were employed in this study to capture the behavior of soils. Refined mesh was set around the caisson shaft with a minimal length of D/60, a minimal length of b/40 for the stiffters, and a minimal length of t/20 for the skirt tip, while the coarse mesh around the far area was set to enhance the efficiency of the calculation. With the installation, the number of mesh elements increased accordingly.

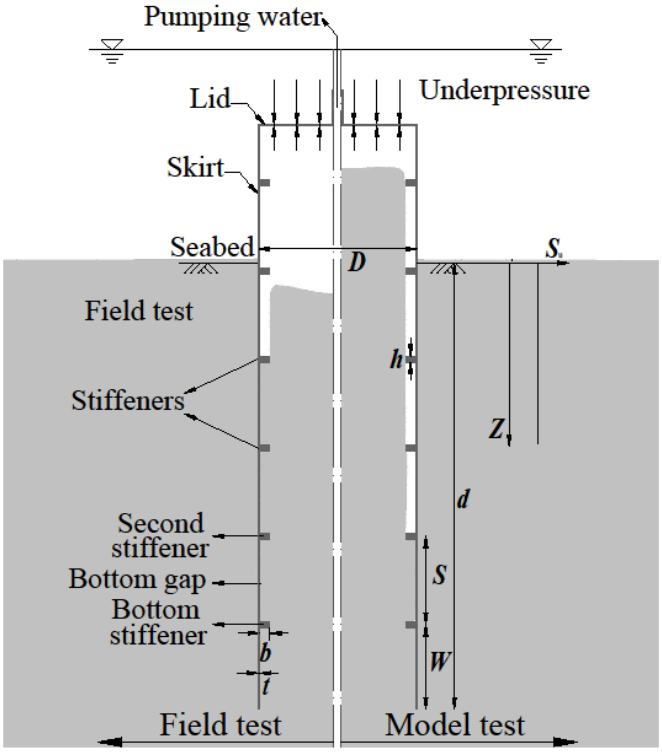


Figure 1. Schematic diagram of stiffened caisson installation in uniform clay.

Tresca yield criterion was chosen to model the behavior of the soil as a linear elastic/perfectly plastic material. Young's modulus (E) and Poisson's ratio (ν) were chosen to

simulate the elastic behavior. The plastic parameters are friction angle and dilation angle (ϕ and ψ). The friction and dilation angle were employed to capture the elastic response, with the aim of describing the plastic response at failure state. The undrained shear strength of clay (S_u) was used in the model, with which the yield surface of the soil was defined. A uniform stiffness ratio of $E/s_u = 500$ was adopted to describe a common soil profile. A Poisson's ratio of $\nu = 0.49$ was employed to simulate the undrained condition for the clay, due to its lower permeability and fast construction speed, while the friction and dilation angles $\phi = \psi = 0$. The geostatic stress conditions were modelled using $K_0 = 1$.

The calculation model used a two-dimensional axisymmetric model. The width and height of the soil boundary in the model were more than ten times the caisson diameter to prevent boundary effects. The surrounding boundaries and the upper and lower boundaries of the model were, respectively, the hinge constraint and rolling constraint. The model mesh type used triangular elements with six-nodes, each having three Gaussian integration points. The contact interface between the structure and the clay was simulated employing a shared node contact unit. This model assumes that the caisson is a rigid structure; the limiting anti-skating strength in contact region was αS_u. The details of the mesh of the model are displayed in Figure 2; D = 4 m, t = 0.05 m, the initial penetration depth was 0.02 m, and the model boundary was 50 m × 50 m.

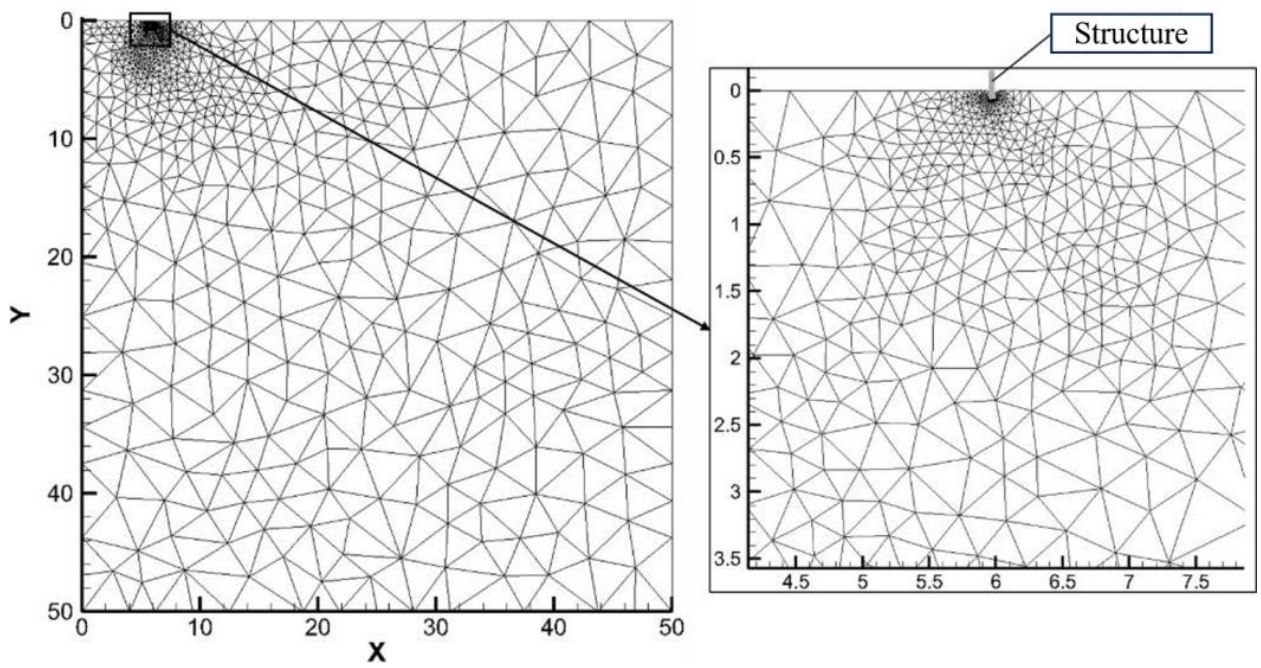
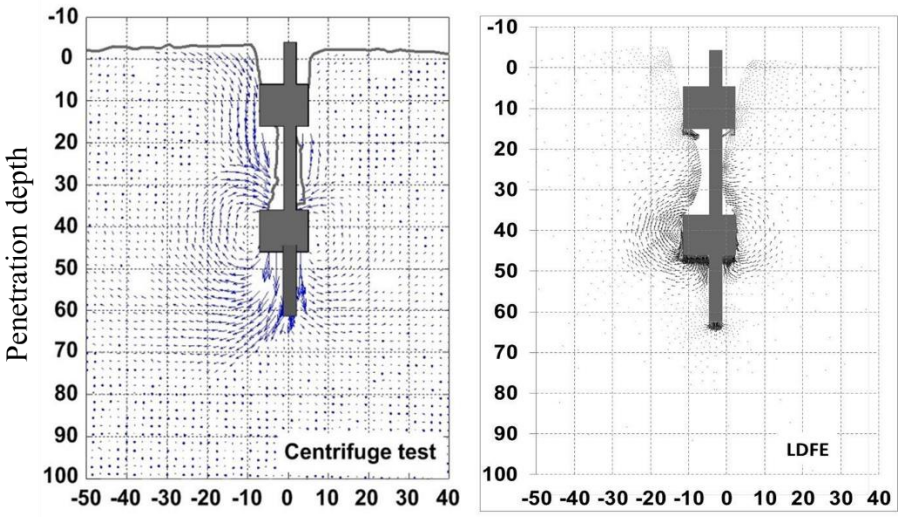


Figure 2. Initial mesh of the model.

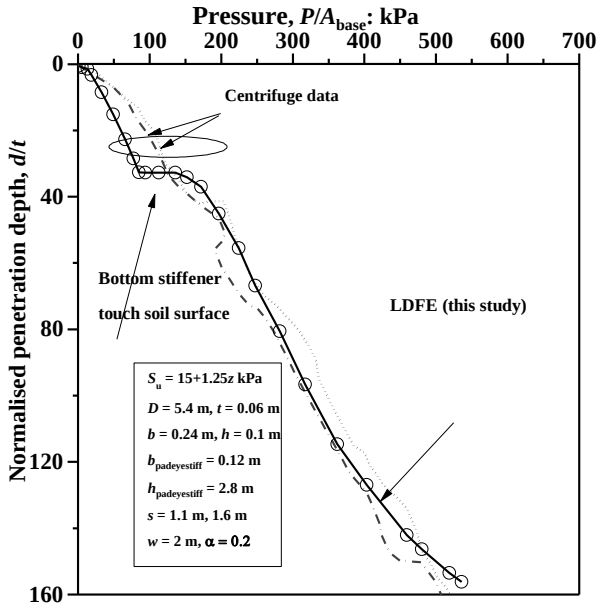
3. Validation

The results from LDFE analyses were validated against data regarding the surrounding soil flow and the obtained penetration resistance during caisson penetration. Model tests in a drum centrifuge at an enhanced gravity of 25× g and 100× g were conducted by Hossain et al. [9], involving a rigid skirt-plate with dimension of 134 mm × 79 mm, assembled with stiffeners on each side. The caisson was installed adjacent to the viewing window of the strongbox, allowing for direct observation of the soil flow around the structure. The experiments were performed in uniform clay (S_u = 12 kPa) with γ' = 7.25 kN/m. Stiffeners were fixed on every side of the skirts with geometrical parameters b/t = 2.0 and 4.0, s/h = 2.0, w/b = 2.7, and 5.3. Two cases were conducted with identical caisson dimensions and soil materials in the centrifuge tests (taking α = 0.3). These tests were carried out with a penetration rate of 1 mm/s, ensuring undrained behavior. A comparison of the surface

heaves and soil flow patterns between RITSS and centrifuge tests is shown in Figure 3a; good agreement was obtained.



(**a**)



(**b**)

Figure 3. Validation of LDFE results with existing test results; (**a**) Comparison of the soil-flow mechanism with centrifuge test result, presented by Hossain et al. (2012) (plan strain); (**b**) Comparison of penetration resistance between LDFE analysis and centrifuge test results, reported by Randolph et al. (1998).

There are almost no prototype measurement or centrifuge model test data concerning the installation resistance of a caisson driving into homogeneous soil. Thus, the installation resistance of a caisson in nonhomogeneous soil calculated using numerical software was in contrast with the existing centrifuge model data [14]. A stiffened caisson with D = 5.4 m was employed in the test and the strength of the clay was expressed as S_u = 15 + 1.25 z kPa ($S_{um}/\gamma' D$ = 0.48 kN/m). There were four groups of inherent stiffeners and parameters, including s/h = 11, b/t = 4.0, w/b = 5.33, and a pad-eye reinforcement with $b_{pad\text{-}eyestiff}$ = 0.12 m, $h_{pad\text{-}eyestiff}$ = 2.8 m. An RITSS analysis was undertaken with identical material to the centrifuge

data (adopting $\alpha = 0.3$). Figure 3b displays the RITSS results of normalized penetration depth d/t compared with the centrifuge test and the relationship between penetration resistance P/A_{base}; as shown, good agreement was obtained.

4. Results and Discussion

Parametric analyses were conducted varying (1) the normalized soil strength, $S_u/\gamma' D$ (varying S_u and D respectively), (2) the ratio of the stiffener width to the skirt thickness, b/t, (3) the ratio of the stiffener interval to the height, s/h, and (4) the friction coefficient between structure and soil, α.

Various factors may have impacted the penetration resistance and soil-flow patterns, i.e., $S_u/\gamma' D$, b/t, s/h (α will only influence the penetration resistance), resulting in the difference between the model test and the prototype. Thus, the model test cannot be widely applied to the practical engineering, especially for the quantitate value of the penetration resistance of a caisson. See Table 1.

Table 1. Summary of the main conversion coefficients in the similarity principle.

Conversion Coefficients	Notation	Expression	Value
Geometry conversion coefficient	C_L	L_P/L_m	n
Geometry conversion coefficient	C_γ	γ_P/γ_m	1
Poisson's ratio conversion coefficient	C_ν	ν_P/ν_m	1
Modulus conversion coefficient	C_E	E_P/E_m	n (=C_L C_γ)
Internal friction angle conversion coefficient	C_φ	φ_P/φ_m	1

4.1. Characteristics during the Installation of Prototypes and Model Tests

To illustrate various characteristics and the differences they induced in the soil-flow patterns and penetration resistance between the prototype and model test, two tests were conducted, varying caisson diameter D from 0.4 m to 4 m with S_u = 5 kPa, b/t = 5, s/h = 11.76, and α = 0.2, in order to simulate a typical prototype (D = 4 m) and undertake a model test with identical geometry in an undisturbed soil sample (D = 0.4 m). Some characteristics of soil flow are relevant to the installation (Figure 4a): (1) Soil flow took place in the stiffener at the bottom and the skirt tip during the initial installation, and the flow trend at the bottom stiffener presented in an upright direction relative to the ground; (2) The heave of the soil surface and soil flow was more significant inside the caisson based on the presence of stiffeners and their interval, while the soil outside of the caisson was generally undisturbed. This conclusion is consistent with the result from LDFE about a caisson penetrating into nonhomogeneous clay with stronger upper soil [15]; (3) With the process of penetration, the soil located in the bottom stiffener flowed around it, with the soil above the stiffener flowing back down to the gap. The position of the base of the bottom stiffener was defined as the ultimate rotation soil flow depth (H_r) around the stiffener at the bottom. Hereafter, the spacing at the bottom was gradually filled with the deeper installation of the caisson; and (4) For all stiffeners except the bottom one, only the depth of the base reached the critical cavity depth, as soil around and above it flowed back into the gap above the stiffener; otherwise, it would have kept forming a cavity. These above four conclusions are consistent with the results of Zhou et al. [10] for a caisson penetrating into nonhomogeneous clay with stronger upper soil.

In both prototype and model tests, when the bottom stiffeners came into contact with the soil surface, the soil under the bottom stiffener had the tendency of effect a rotating failure, and the soil above it flowed upright to the surface. In the prototype, when penetration depth d/D = 1 and the penetration depth of the bottom stiffener d/D = 0.45, the surrounding soil at bottom stiffener rotated before flowing into the gap; the same occurred at the normalized penetration depth d/D = 2.4 and normalized penetration depth of the bottom stiffener d/D = 1.8 in the model test (see Figure 4b). Similarly, backflow occurred

when the penetration depth of the second bottom stiffener was d/D = 0.5 in the prototype and when the penetration depth of the second bottom stiffener d/D = 1.7 (Figure 4b) in the model test. The soil heave height in the model test was about three times that used in the prototype.

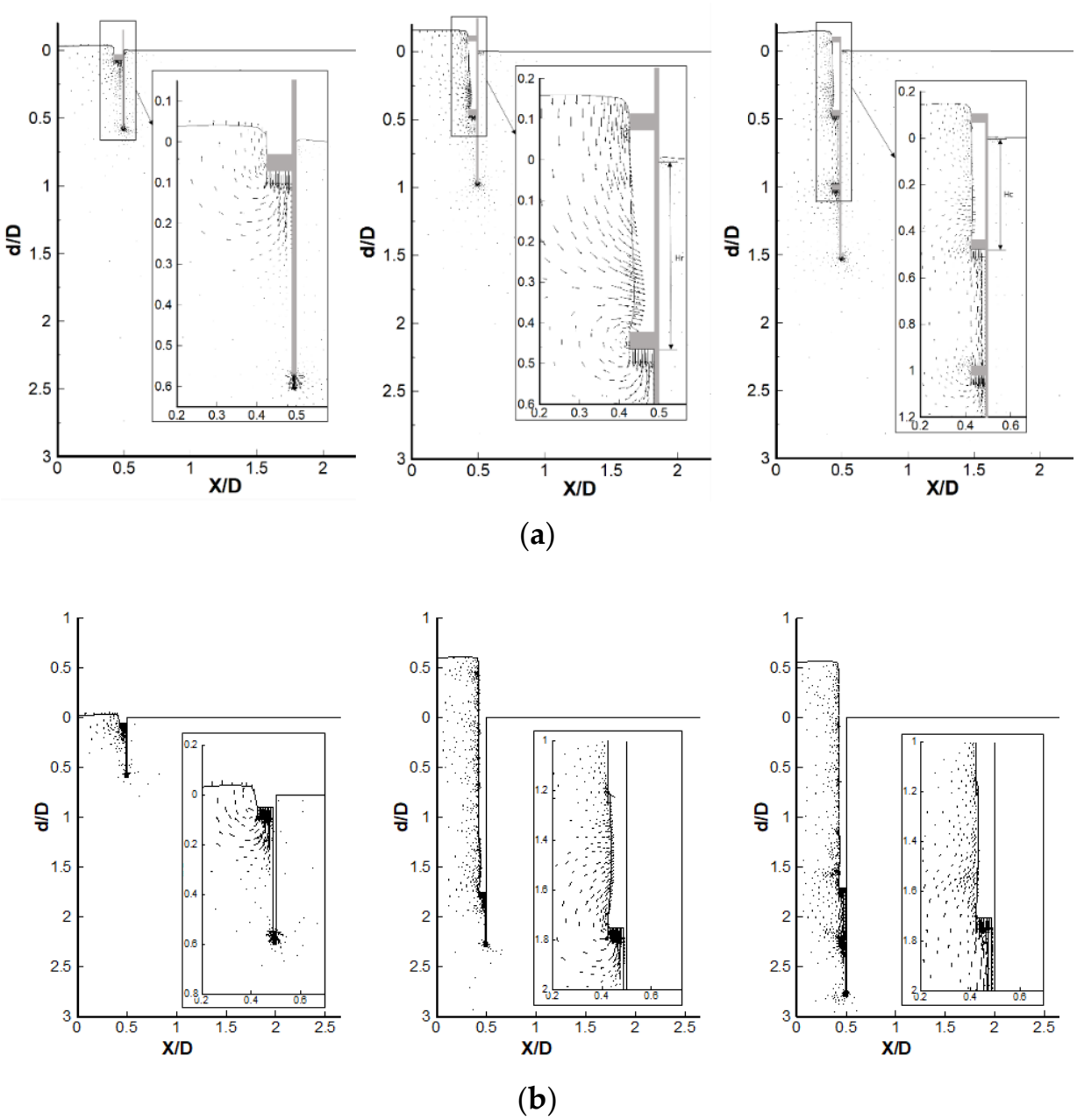


Figure 4. Difference in soil-flow mechanisms during installation between a prototype test and a model test; (**a**) Caisson in prototype test; (**b**) Caisson in model test.

The difference of soil flow was also reflected in penetration resistance (Figure 4b). There was some overlap between the curves at penetrating depth $d/D < 0.45$, because the skirt and stiffener at the bottom penetrated into the clay during the initial penetration, and the bearing capacity coefficient after normalization is independent on soil strength. In the prototype, the second mutation occurred when penetration depth d/D = 1, when the soil flowed back to the bottom gap; the same occurred with a penetration depth of d/D = 2.4 in the model test. The third mutation occurred when penetration depth d/D = 1.5, when the soil flowed back to the second bottom gap; the same thing occurred

when the penetration depth d/D = 2.9 in the model test. This is completely consistent with the soil flow described above. The backflow of soil in the gap of any layer is accompanied by a mutation in the penetration resistance, because the original cavity is gradually filled, there is friction resistance between the skirt inner wall and soil, and the end resistance of the upper and lower stiffener surface are added to the component of penetration resistance. The maximum difference in penetration resistance between the prototype and model may be 1.7-fold.

It can be seen that even if undisturbed soil is used and the geometric shape of the model is completely consistent with the prototype, the size effect has a significant impact on the simulation results of soil flow in the model test, with seriously lagged soil backflow appearing, affecting the penetration resistance. It is therefore significant to study the difference and the transformation mode between model tests and prototypes. Compared with the results between the case in the prototype tests and in $1\times g$ model tests, it can be concluded that the soil flow mechanism was significantly different to that induced by the differential flow pattern around the stiffener, as shown in Figure 4a,b, which affected the penetration resistance. To obtain accurate results for penetration resistance, interpretation of the data of $1\times g$ model tests is required.

4.2. Parametric Study on Small Scale Model Caissons

4.2.1. The Effect of the Model Scale with Various Soil Strength (S_u)

To investigate the effect of soil strength on the soil-flow mechanisms and penetration resistance, a group of analyses were carried out at soil strength S_u = 5, 10, and 15 kPa, with identical D = 4 m, b/t = 5, s/h = 11.76, α = 0.2. The effect of the model size with different shear strengths of clay on the soil-flow pattern within the caisson at a penetrating depth of 2.25 are plotted in Figure 5a.

In homogeneous clay with a lower shear strength (S_u = 5 kPa, $S_u/\gamma' D$ = 0.21), since the soil rotationally flowed around the bottom stiffener, the space at the bottom was largely filled by the backflow soil, and the soil at the bottom stiffener continued to flow into the void above it. The bottom second stiffener scraped the nearby soil into the gap below it, and the soil above it flowed vertically upward to the ground, forming a cavity.

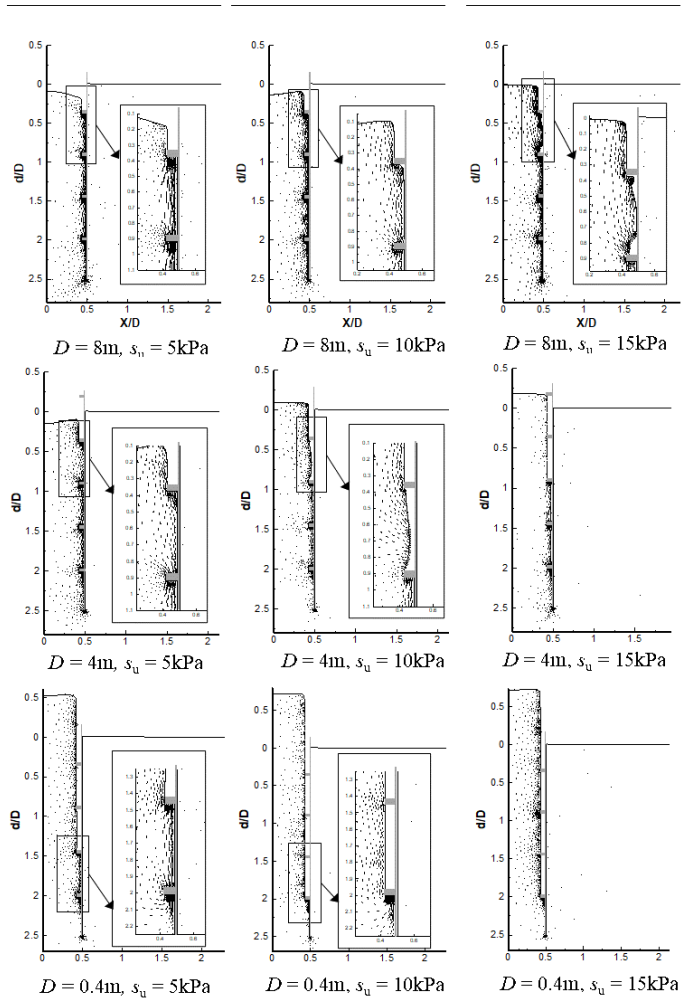
For the case with a higher soil strength of S_u = 10 kPa ($S_u/\gamma' D$ = 0.43, Figure 5), the soil began to rotate along the bottom stiffener and flow into the bottom gap. The soil above the second stiffener remained upright, forming a cavity with the caisson wall. The soil heave height inside the caisson was about 2.5 times that of the case, as shown in Figure 5.

It can be concluded that for both prototype and model tests, the higher the soil strength, the slower the soil backflow, making it easier to maintain the vertical wall of soil between the stiffeners. If the penetration depth is large enough, the soil will rotate along the bottom stiffener and backflow into the gap above it. These effects of soil strength are consistent with the results obtained by Zhou et al. [10] in their study of stiffened caissons in non-homogeneous clays and by Hossain et al. [9] in their centrifuge tests.

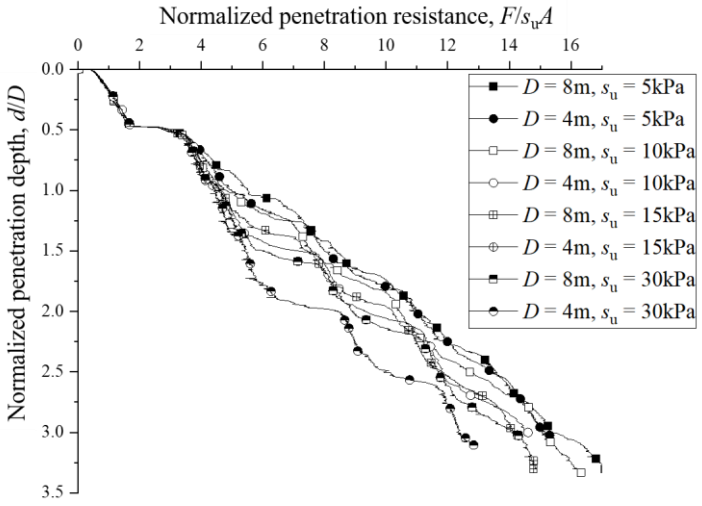
For the lowest $S_u/\gamma' D$, ($S_u/\gamma' D$ = 0.21, S_u = 5 kPa), the soil started to fill the third gap in the prototype while the soil almost filled the first gap in the model test. When $S_u/\gamma' D$ = 0.42 (S_u = 10 kPa), the bottom two gaps were completely filled by the backflow soil, with soil reflux taking place in the third gap in the prototype. In the meantime, the soil above the bottom stiffener had no tendency to backflow in the model test. For the highest $S_u/\gamma' D$ ($S_u/\gamma' D$ = 0.63, S_u = 15 kPa), the bottom two gaps filled with soil and the soil above the third stiffener flowed vertically upward to the ground, forming a cavity in the prototype, while the soil above the bottom stiffener flowed vertically in the model test.

It can be concluded that for both the prototype and model test, the higher the soil strength, the slower the soil backflow, and hence, the easier it is to keep the soil wall between the stiffeners vertically. These effects of soil strength are consistent with results obtained by Zhou et al. [10] in their study of stiffened caissons in non-homogeneous clays, and observations following centrifuge tests by Hossain et al. [9]. Under the geometric scale

mentioned above (D_p/D_m = 10), the soil flow condition in the model test lagged behind that in the prototype test by at least two gaps (1*D*).



(**a**)



(**b**)

Figure 5. Difference in soil flow pattern and penetration resistance between the prototype test and model tests; (**a**) Soil flow patterns with varying S_u; (**b**) Penetration resistance with varying S_u.

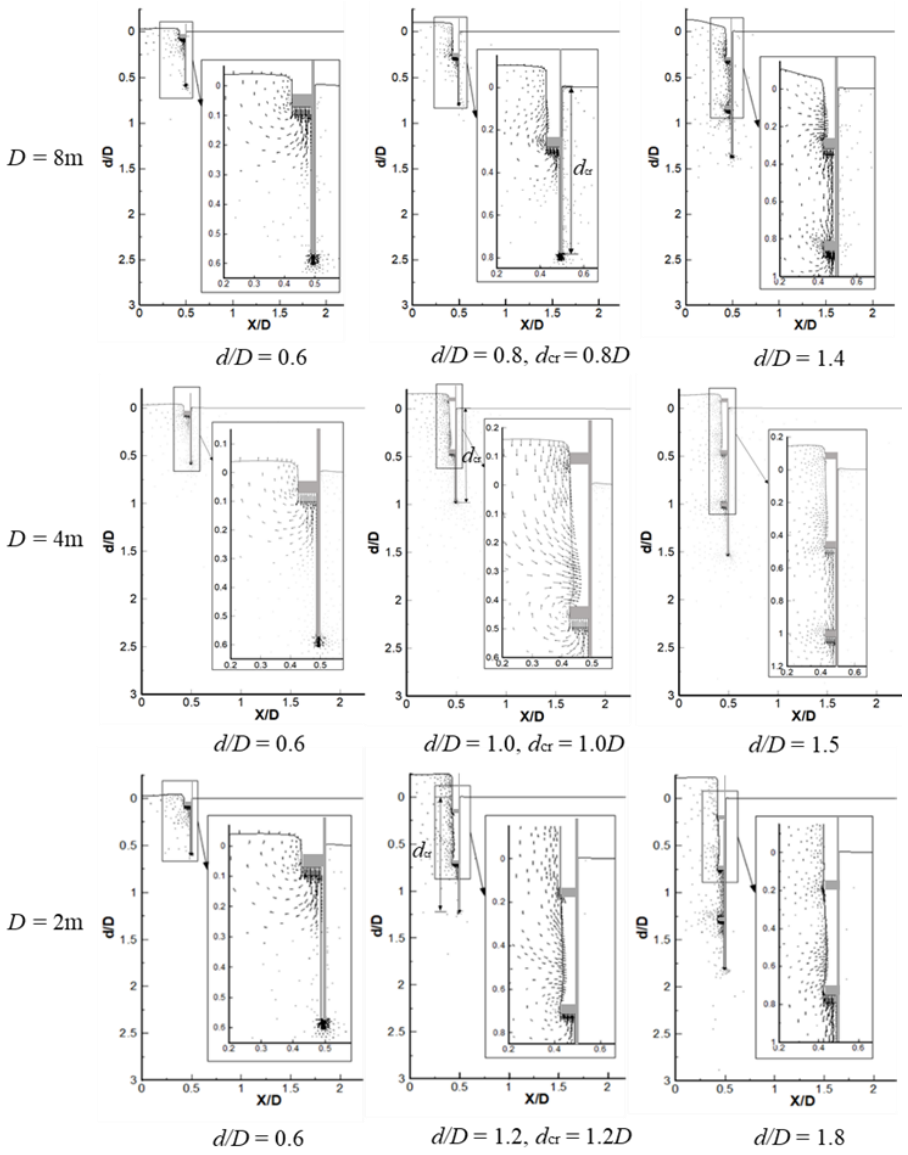
In terms of soil heave inside the caisson, when S_u is small (S_u = 5 kPa), the normalized soil heave height of the model test was 0.6D larger than that of the prototype which was 0.75D when S_u = 10 kPa and 0.95D when S_u = 15 kPa. With all other conditions the same, the normalized soil heave height in the model test was generally higher than that in the prototype, and the bigger the S_u, the greater the difference between the model and the prototype.

The influence of model scale with different normalized soil strengths on penetrating resistance are plotted in Figure 5b (S_u = 5, 10 and 15 kPa). There was overlap between the curves at a penetration depth of $d/D < 0.45$, which has been explained above. The curves stayed consistent until soil backflow happened, as in $S_u/\gamma' D = 0.21$ (S_u = 5 kPa, D = 4 m). With installation depth $d/D > H_r/D$, for the equivalent diameter of the caisson, the lower the S_u, the higher the bearing capacity coefficient. The degree of cavity formation varied with soil strength, and backflow occurred at different H_c and H_r, resulting in different soil uplift heights and leading to different penetration resistance mechanisms. The bearing capacity coefficients of the three mutated at different depths; the change law was consistent with the soil flow law mentioned above. For the cases with S_u = 10 kPa and S_u = 15 kPa, the bearing capacity coefficients of the model test were 4.3 times larger than those of the prototype, which was four times that of the case with S_u = 5 kPa. To investigate the penetration depth of ship anchors in clay sediment, physical and numerical simulations were performed by Han et al. [16]. In their study, undrained shear strength was considered the main factor affecting the penetration resistance of the anchor. Additionally, the penetration depth was decreased as S_u increased, which indicated that a larger penetration resistance for the anchor had been obtained, which is consistent with the conclusions in this study. It can be seen that there was a huge difference between the penetration resistance of the model and that of the prototype.

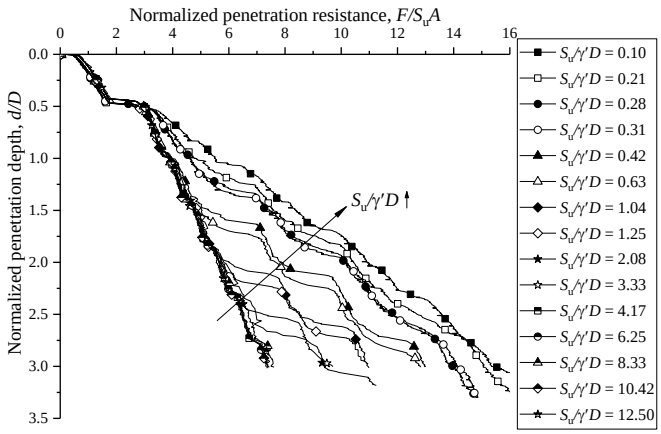
4.2.2. Effect of the Model Scale with Various Diameters of Caisson (D)

The installation resistance and soil failure patterns are displayed in Figure 6 to reveal the influence of the size of caisson (with D = 4, 2, 1, 0.4 and 0.2 m) with identical soil strength S_u = 10 kPa (b/t = 5, s/h = 11.76, α = 0.2). For a larger diameter (D = 4 m), the bottom two gaps were completely filled by the backflow soil at d/D = 2.25, with the soil at the third stiffener continuing to flow into the gap above it, filling the gap gradually, while the soil only just began to flow into the bottom gap. For the smaller diameter D = 0.4 m, the soil above the bottom stiffener was just beginning to fail, flowing into the bottom gap. For D = 0.04 m, the soil did not flow back and completely filled the gap between the inserted stiffeners, albeit while standing vertically, indicating no collapse. This suggests that the lateral pressure is lowered by a smaller caisson diameter, resulting in a delay of soil backflow into the gaps and leading to a higher soil heave height. For D = 0.4 m and D = 0.04 m, the surface was heaved by 0.6D, which increased significantly to 0.05D for D = 4 m, as shown in Figure 6a.

The curves coincided when no backflow occurred. As backflow occurred in each case, the curves dispersed one by one. The soil flow mechanism explained above was consistent with the changes in penetration resistance. When soil back flow occurred in the coverage area of the instant penetration depth, the larger the size, the bigger the penetration resistance, and the earlier the soil backflow occurs. When the model size was small and the penetration depth did not reach H_r, the penetration resistance was independent of the diameter. The results show that, with a normalized shear strength increase, less soil flowed back into the gap between the stiffeners, and hence, lower penetration resistance was obtained. During the first stage of the penetration, no soil flow was observed, and hence, no differences in resistance were observed. This indicates that traditional 1 g model tests with pipe piles may yield better results than in prototype tests, especially for soil patterns.



(**a**)



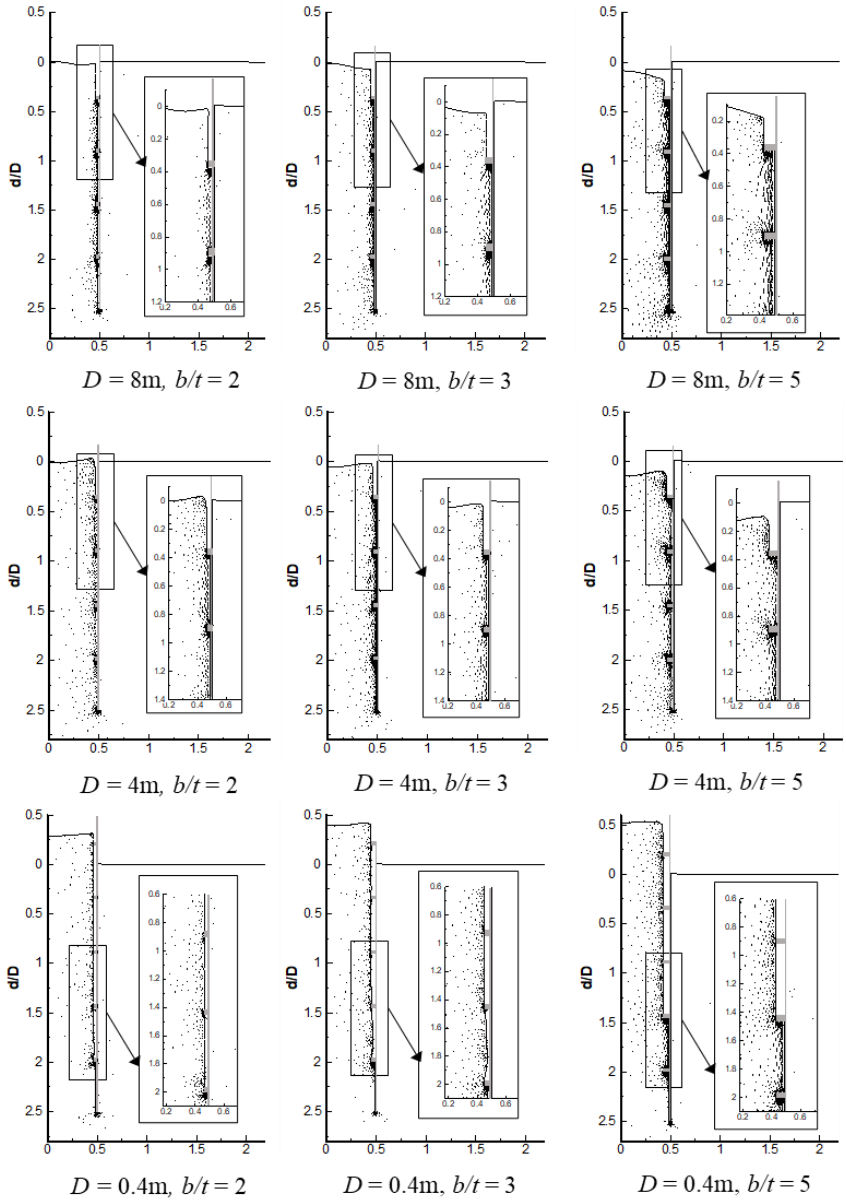
(**b**)

Figure 6. Effect of normalized soil strength on penetration resistance; (**a**) Soil flow patterns with varying *D*; (**b**) Penetration resistance with varying *D*.

4.2.3. Effect of the Model Scale with Various Stiffener Widths (b/t)

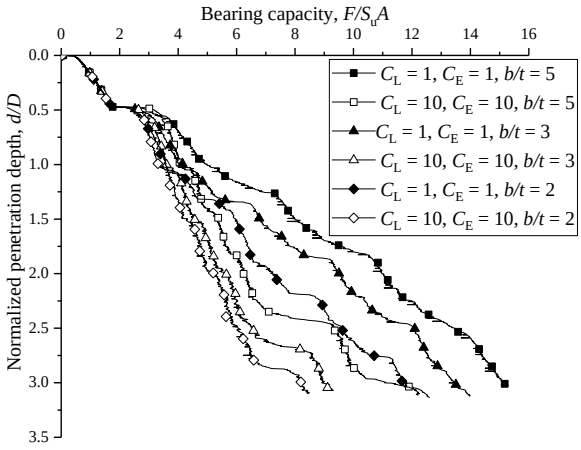
A series of prototype and model tests with various stiffener width profiles were conducted to examine the impact of the effects of reduced scale on the installation mechanisms.

Figure 7 shows the soil failure pattern for b/t = 5, 3, and 2 in model tests and in the prototype (D = 4 and 0.4 m, S_u = 10 kPa, s/h = 11.76, α = 0.2). At the normalized penetration of d/D = 2.505 (four stiffeners were embedded in the clay), the bottom three gaps were completely filled by the backflow soil in all three prototypes and the soil above the fourth stiffener remained upright, flowing vertically to the surface. In the tests with the identical penetration depth, when b/t = 2, the soil above the bottom stiffener did not return; when b/t = 3, the soil above the bottom stiffener failed and began to return to the interval; and finally, when b/t = 5, the bottom gap was completely filled with the returning soil while the soil above the second stiffener remained upright.



(**a**)

Figure 7. *Cont.*



(**b**)

Figure 7. Effect of the model scale varying with stiffener width on penetration resistance (C_E = 1 and 10, C_L = 1 and 10, s/h = 11.76, α = 0.2, b/t = 5, 3, 2); (**a**) Soil flow patterns with varying b/t; (**b**) Penetration resistance with varying b/t.

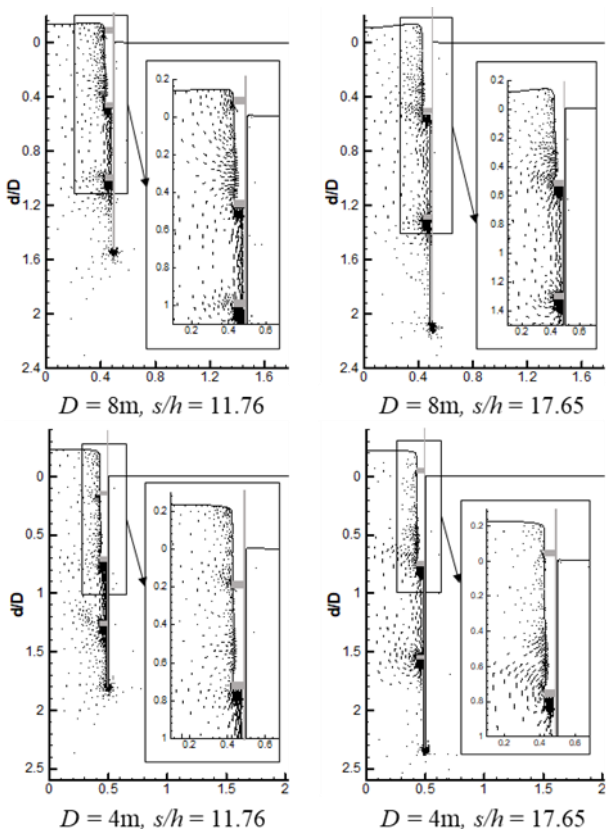
The impact of the stiffener width on soil flow in the model and prototype was found to be basically the same. With an increase in stiffener width, the stiffener volume and intervals increased and the faster the soil mass flowed back into the gap, due to the greater lateral pressure caused by the greater heave height, making the soil strength unable to maintain the verticality of the wall. For b/t = 2.0, soil disturbance mainly occurred around stiffener and at the bottom of caisson skirt, while the displacement of soil in other positions was much smaller than that in the other two groups. In conclusion, in homogeneous clay, the influence of the width of the stiffener on the soil flow mechanism of the soil mass during the penetration of both the prototypes and model tests was the same: (1) the larger the width of the stiffener, the greater the disturbance of the stiffener on the surrounding soil and the larger the disturbance range; and (2) the larger the stiffener width, the higher the level of the soil inside the caisson and the sooner the soil backflow occurs. These conclusions are in excellent agreement with those obtained by Hossain et al., who used a centrifugal test in homogeneous clay.

With regard to the heave of the soil surface inside the caisson, when b/t = 2, 3, and 5, the uplift height of the soil in the caisson of the model test was 0.26D, 0.47D, and 0.72D higher than that of the prototype, respectively. Based on the above phenomena, it can be concluded that the greater the stiffener width, the larger the difference in the soil flow mechanism between the model test and the corresponding prototype.

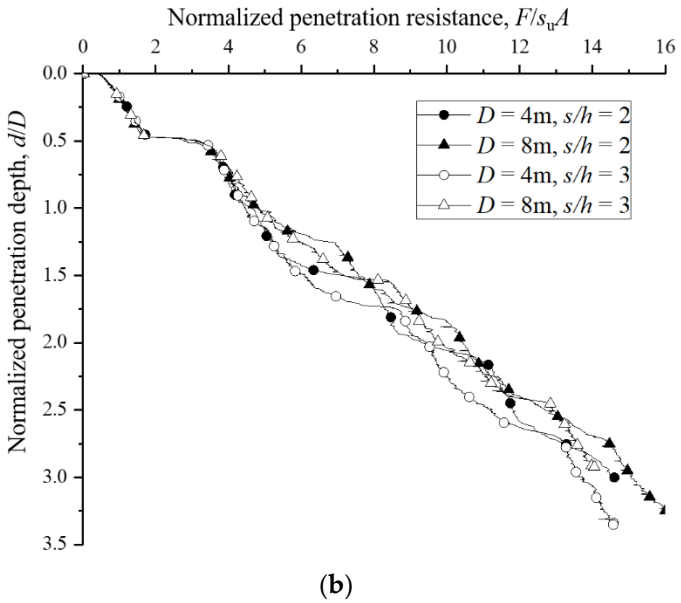
The influence of model scale on penetration resistance with various stiffener widths is plotted in Figure 7. With a penetration depth $d/D > 0.45$, as the stiffener width increased, the bearing capacity coefficient increased and the faster each curve mutation occurred, which means the faster the soil flow occurs. This is consistent with the soil flow law obtained above. For b/t = 5, the bearing capacity coefficients of the model test were 26.6% less than those of the prototype, i.e., 34.1% when b/t = 3 and 2. It can be seen that a significant difference existed between the penetration resistance of the model test and the prototype, and that this increased with the width of the stiffener. The results show that, with different scales and percentages of following the similarity principle, the modification methods were different in the various cases in the 1 g model tests.

4.2.4. Effect of the Model Scale with Various Spacings between the Stiffeners and Interface Friction Coefficient (s/h and α)

To examine the impact of model scale on the installation mechanism by varying the stiffener spacing, several tests were carried out, i.e., s/h = 11.76 and 17.65 with D = 4 and 0.4 m, S_u = 10 kPa (b/t = 5, α = 0.2). The different penetration resistances are shown in Figure 8.



(**a**)



(**b**)

Figure 8. Effect of model scale varying with the interface friction coefficient on the penetration resistance in the prototype and model tests (D = 4 and 8, s/h = 2 and 3); (**a**) Soil flow patterns with varying s/h; (**b**) Penetration resistance with varying s/h.

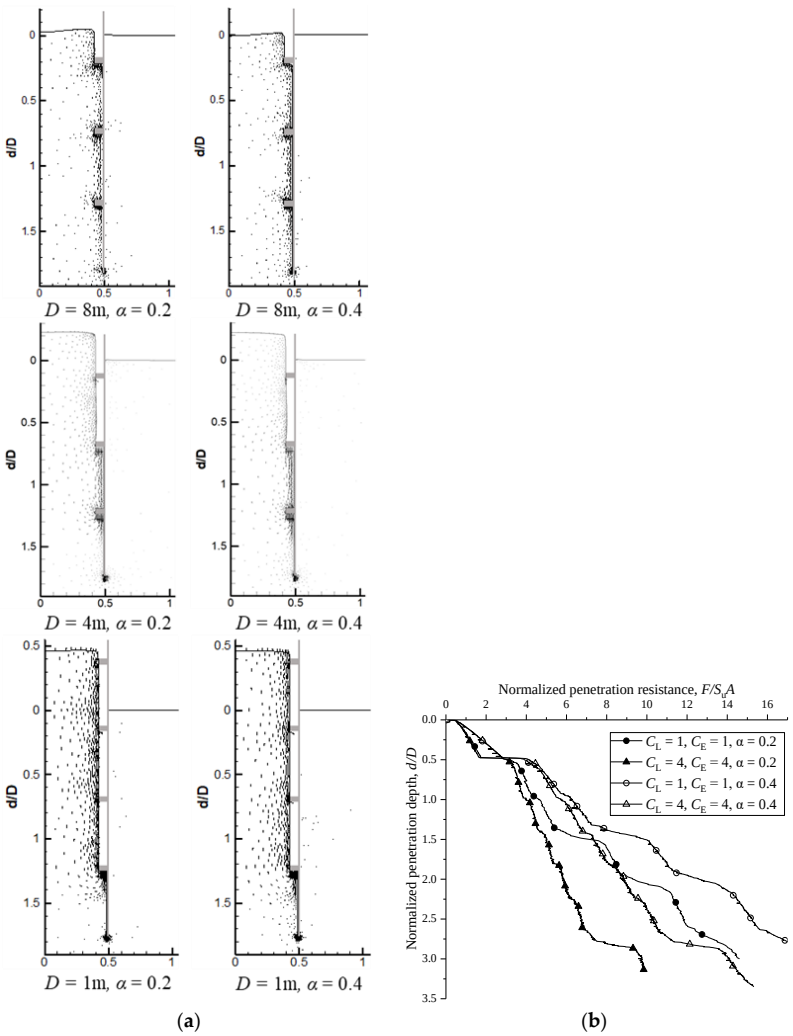
The soil above the second stiffener of the caisson with small spacing (s/h = 11.76) flowed back at the penetrating depth of the second stiffener $d2nd/D$ = 0.73 in the prototype, which was 2.2 in model test. For cases with large spacing (s/h = 17.65), soil backflow did not occur until $d2nd/D$ = 0.77 in the prototype or $d2nd/D$ = 2.87 in model test (see Figure 8). With s/h = 11.76, H_c of the case of the model test was 1.47D larger than that of

the prototype, while for the case with s/h = 17.65, H_c of the model test was 2.1D larger than that of the prototype. With a larger s/h, the difference of soil flow between model test and prototype increased.

Therefore, in homogeneous clay, the stiffener spacing of the prototype structure had a significant impact on the soil flow patterns, and the H_c increased as the stiffener spacing increased. In Figure 8, the effect of the model scale with varying s/h was only reflected in the depth of the mutation of N_c; it had basically no effect on the difference in the size of N_c between the two model and prototype groups.

The influence degree on the model and prototype was the same with different s/h. The difference between the model test and the prototype was also very large, but this was basically not related to the change of s/h.

Two interface friction coefficients (α = 0.2 and 0.4) were chosen to measure their impact on a reduced scale installation mechanism, with soil strength and caisson dimension remaining the same as S_u = 10 kPa, D = 4 and 0.4 m, b/t = 5, s/h = 11.76. Similar observations to Figure 9, with different α between the model test and prototype, were obtained. The difference in the soil flow mechanism between the two groups was consistent with varying α; this revealed that the interface friction coefficient had little effect on the soilflow mechanism. The change of α had basically no effect on the size effect.



(**a**) (**b**)

Figure 9. Effect of model scale with varying interface friction coefficient on penetration resistance in prototype and model tests (C_E = 1 and 4, C_L = 1 and 4, α = 0.2 and 0.4); (**a**) Soil flow patterns with varying α; (**b**) Penetration resistance with varying α.

The bearing capacity coefficients were different with various friction coefficients; the bearing capacity coefficient with a large friction coefficient on the contact surface was higher. In the model and prototype, the trend of the curves was basically consistent, with mutations and fluctuations occurring at the same penetration depth. At a penetration depth of 2.5D, α = 0.2, and 0.4, the bearing capacity coefficient of the model test was 5.1 and 4.9 smaller than that of the prototype, respectively, which was adjacent. It can be concluded that the friction coefficient had no effect on the model scale effect in terms of the flow patterns of soil, and that it also had only a minimal effect on the penetration resistance.

4.2.5. Effect of Model Scale with Various Normalized Soil Strength ($S_u/\gamma'D$)

To explore the effect of model scale on the reduced scale model test for the normalized soil strength profile, a set of cases were selected with normalized soil strength $S_u/\gamma'D$ = 0.21, 0.42, 0.625, 0.83, 1.04, 1.67, 2.08, 2.5, 4.17, 6.25, and 8.33 and with identical b/t = 5, s/h = 11.76, and α = 0.2. The effect of the reduction coefficient on the installation mechanisms of varying the normalized soil strength is plotted in Figure 10. It was found that the soil flow mechanisms of the prototype (D = 4 m) and the reduced scale model test (D = 1 m) with the same normalized soil strength $S_u/\gamma'D$ = 0.83 were generally the same, while that of the reduced scale model test (D = 1 m) with different strength $S_u/\gamma'D$ = 1.67 was quite different. At a penetration of d/D = 2.2, the bottom gaps in the two cases with $S_u/\gamma'D$ = 0.83 were completely filled with backflow soil and the soil above the second stiffener flowed downward into the second bottom gap. For $S_u/\gamma'D$ = 1.67, soil backflow barely occurred in the bottom interval, while the soil above the second one did not tend to flow back into the second gap, instead maintaining a vertical wall and flowing toward the surface. The surface was heaved by 0.25D for $S_u/\gamma'D$ = 0.83, which increased to 0.4D for $S_u/\gamma'D$ = 1.67. With the process of penetration, at a penetration of d/D = 2.985, the bottom two gaps were filled with backflow soil and part of the soil was scraped into the gap by the fourth stiffener for both $S_u/\gamma'D$ = 0.83 and $S_u/\gamma'D$ = 1.67. The soil inside the caisson flowed downward, filling the third gap gradually for $S_u/\gamma'D$ = 0.83, but for the higher $S_u/\gamma'D$ = 1.67, the soil did not flow back into the third gap. The soil heave height inside caisson increased with increasing normalized soil strength, i.e., about 0.1D and 0.3D for $S_u/\gamma'D$ = 0.83 and $S_u/\gamma'D$ = 1.67, respectively.

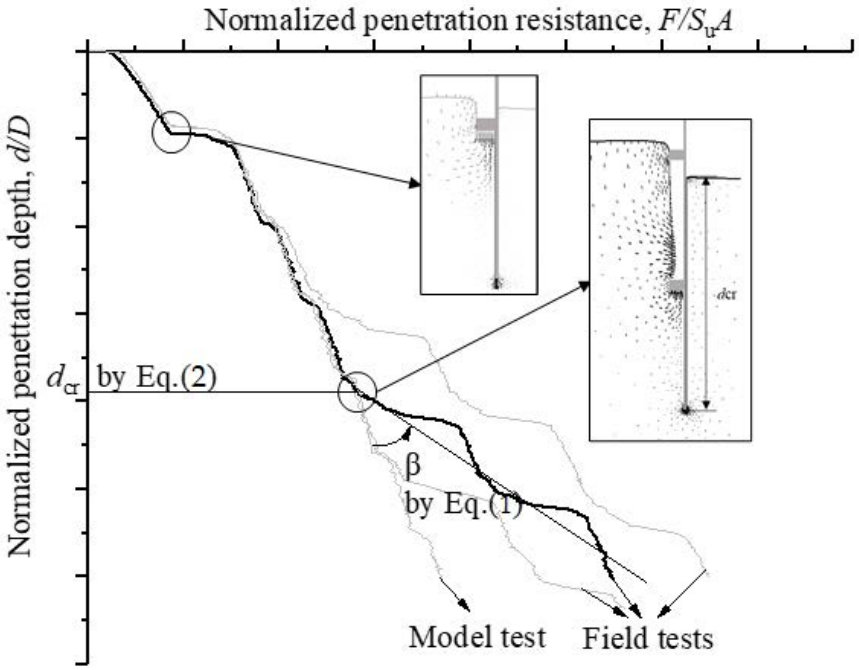


Figure 10. Mechanism of penetration depth.

It can be concluded that in homogeneous clay, stiffened caissons with the same shape and different sizes penetrating into clay with the same normalized soil strength showed consistent soil flow mechanisms. Ideally, the soil flow mechanism during pile sinking can be completely simulated in the laboratory.

Even if the size of the caisson and the soil strength are not equal, the cases with identical normalized soil strength (i.e., when the similarity principle was satisfied) showed basically identical bearing capacity coefficients during installation (see Figure 10). The FE results of normalized soil strength ($S_u/\gamma' D$ = 0.10, 0.21, 0.28, 0.31, 0.42, 0.63, 1.04, 1.35, 2.08, 3.33, 4.17, 6.25, 8.33, 10.42, and 12.50) with b/t = 5, s/h = 11.76, α = 0.2 are shown in Figure 11. It can be concluded that the installation resistance varied with the normalized soil strength, i.e., the higher the $S_u/\gamma' D$ (higher S_u or smaller D), the greater the penetration resistance, requiring larger force during installation.

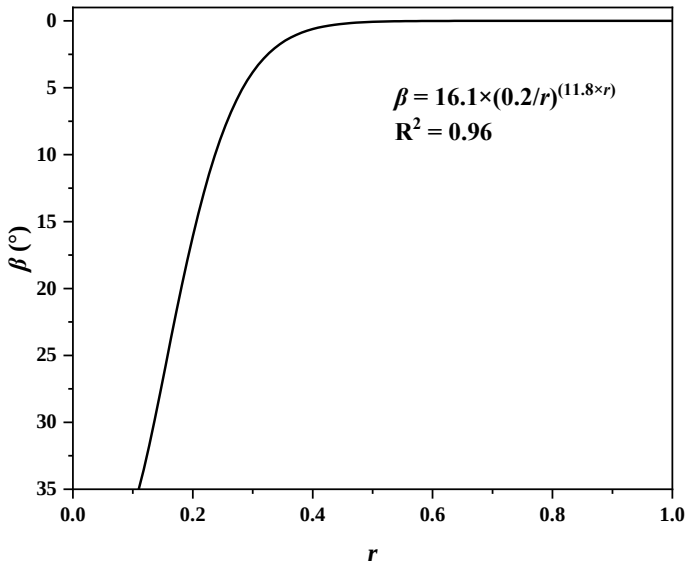


Figure 11. Penetration resistance—predicted model of stiffened caisson based on 1 g model test.

4.2.6. Predicting Prototype Installation Resistance Based on 1 G Model Test

According to the above discussion, two parameters ($S_u/\gamma' D$, b/t and α) had striking effects on the mechanisms of caissons installation in both the model test and prototype. The model test can easily be adjusted to control the friction coefficient such that it is identical to that in prototype, and more for α = 0.2. In order to establish the relationship between the installation resistance of the caisson in the prototype and in the 1 g model test, formulas are put forward with varying $S_u/\gamma' D$ and b/t.

Based on the failure mechanisms during the installation of a caisson in clay in the 1 g model tests and prototype, an installation resistance for a stiffened caisson penetrating clay is proposed, as shown in Figure 11, in which a rotational angle from the resistance of the model test data to the prototype was obtained from Equation (1) and the separation point was determined using Equation (2). Both of these equations were obtained from data fitting based on numerous data from large deformation finite element analysis

$$\beta = 16.1 \times \left(\frac{0.2}{r}\right)^{\left(\frac{11.8}{r}\right)} \quad (1)$$

$$\frac{d_{cr}}{D} = \left(1.85 - 0.12\frac{b}{t}\right)\left(\frac{S_u}{\gamma' D}\right)^{0.44} + \frac{w}{D} \quad (2)$$

where r is $S_u/\gamma' D$ in the 1 g model test divided by $S_u/\gamma' D$ of prototype, b is the stiffener width, t is to the wall thickness of the caisson, D is the caisson diameter, w is the bottom

spacing between the caisson and the stiffener, and S_u is the undrained shear strength of the clay.

5. Concluding Remarks

This study, undertaken through large deformation finite element analysis, explored the inner mechanisms of the difference between model tests and prototype tests in terms of different sizes of caissons through systematic research, and identified the factors which determined the observed differences.

(1) Compared with centrifugal model tests, soil backflow for the case of a 1 g model test without applying the similarity principle occurred at larger penetration depths; (2) It was found that $S_u/\gamma' D$, and b/t were the main parameters influencing the factors for the behavior of the caisson in the 1 g model tests and in the prototype; and (3) A method for predicting the installation resistance of a stiffened caisson in clay based on 1 g model tests is proposed, in which an interpretation method from the resistance shown in the model test data compared to that in the prototype is proposed.

Author Contributions: Data curation, S.L.; Writing—original draft, Y.H.; Writing—review & editing, S.H. and M.Z. All authors have read and agreed to the published version of the manuscript.

Funding: This research is supported by National Natural Science Foundation of China (No. 42276213), the fundamental research funds for the central universities (2023ZYGXZR028), Special Fund Project of Six Major Marine Industries in 2022 (GDNRC [2022]27), Shenzhen Steady Support Project for Universities Key program (Grant Number GXWDS20220818152909001).

Data Availability Statement: The data used to support the findings of this study are available from the corresponding author upon request.

Conflicts of Interest: Author Sifen Huang was employed by the Guangdong Shunde Power Design Institute Co., Ltd.; Yuwei Han was employed by Guangzhou Airport Construction Investment Group Co., Ltd. The remaining authors declare that the research was conducted in the absence of any commercial or financial relationships that could be construed as a potential conflict of interest.

Abbreviations

b	width of stiffener
d	penetration depth of stiffened caisson
D	diameter of stiffened caisson
D_m	diameter of stiffened caisson in scaled model
D_p	diameter of stiffened caisson in prototype
C_E	modulus conversion coefficient of similarity principle
C_L	geometry conversion coefficient of similarity principle
C_γ	unit weight conversion coefficient of similarity principle
C_υ	Poisson's ratio conversion coefficient of similarity principle
C_φ	internal friction conversion coefficient of similarity principle
E	Young's modulus of soil
E_m	Young's modulus of soil in scaled model
E_p	Young's modulus of soil in prototype
h	height of stiffener
H_c	limiting cavity depth
H_r	depth of rotation flow
L	length of caisson
s	(edge to edge) spacing between two successive stiffeners
S_u	undrained shear strength of soil
S_{um}	undrained shear strength at mudline
t	thickness of skirt wall
W	distance of bottom stiffener base from skirt tip
z	depth below soil surface
α	coefficient of interface friction

γ	unit weight of soil
γ_m	unit weight of soil in scaled model
γ_p	unit weight of soil in prototype
υ	Poisson's ratio of soil
υ_m	Poisson's ratio of soil in scaled model
υ_p	Poisson's ratio of soil in prototype
φ	internal friction of soil
φ_m	internal friction of soil in scaled model
φ_p	internal friction of soil in prototype

References

1. Ram, S.L.; Mohana, R. Simulation and numerical analysis of offshore wind turbine with monopile foundation. *IOP Conf. Ser. Mater. Sci. Eng.* **2020**, *872*, 012046.
2. Wang, X.; Li, S.; Li, J. Experimental and numerical study on lateral response of pile-group for offshore wind turbines in sand. *Mar. Georesour. Geotechnol.* **2023**, *41*, 524–543. [CrossRef]
3. Alnmr, A.; Mayassah, M. Innovations in Offshore Wind: Reviewing Current Status and Future Prospects with a Parametric Analysis of Helical Pile Performance for Anchoring Mooring Lines. *J. Mar. Sci. Eng.* **2024**, *12*, 1040. [CrossRef]
4. Iai, S. Similitude for shaking table tests on soil-structure-fluid model in 1g gravitational field. *Soils Found.* **1989**, *29*, 105–118. [CrossRef]
5. Molina-Gomez, F.; Caicedo, B.; Viana da Fonseca, A. Physical modelling of soil liquefaction in a novel micro shaking table. *Geomech. Eng.* **2019**, *19*, 229–240.
6. Taylor, R.N. (Ed.) *Geotechnical Centrifuge Technology*; CRC Press: Boca Raton, FL, USA, 2018.
7. Dendani, H. Suction anchors: Some critical aspects for their design and installation in clayey soils. In Proceedings of the Offshore Technology Conference, Houston, TX, USA, 5–8 May 2003; p. OTC-15376.
8. Park, S. Installation and Operation of Suction Caisson Anchors in Calcareous Sand. Doctoral Thesis, The University of Western Australia, Perth, Australia, 2023.
9. Hossain, M.S.; Lehane, B.M.; Hu, Y.; Gao, Y. Soil flow mechanisms around and between stiffeners of caissons during installation in clay. *Can. Geotech. J.* **2012**, *49*, 442–459. [CrossRef]
10. Zhou, M.; Hossain, M.S.; Hu, Y.; Liu, H. Installation of stiffened caissons in nonhomogeneous clays. *J. Geotech. Geoenviron. Eng.* **2016**, *142*, 04015079. [CrossRef]
11. Faizi, K.; Faramarzi, A.; Dirar, S.; Chapman, D. Development of an analytical model for predicting the lateral bearing capacity of caisson foundations in cohesionless soils. *Ocean Eng.* **2020**, *218*, 108112. [CrossRef]
12. Faizi, K.; Faramarzi, A.; Dirar, S.; Chapman, D.; Cui, G.; Heron, C.M.; Marshall, A.M. Assessing the performance of winged caisson foundations for offshore wind turbines. *Mar. Georesour. Geotechnol.* **2024**, *42*, 289–304. [CrossRef]
13. Hu, Y.; Randolph, M.F. A practical numerical approach for large deformation problems in soil. *Int. J. Numer. Anal. Methods Geomech.* **1998**, *22*, 327–350. [CrossRef]
14. Randolph, M.F.; O'neill, M.P.; Stewart, D.P.; Erbrich, C. Performance of suction anchors in fine-grained calcareous soils. In Proceedings of the Offshore Technology Conference, Houston, TX, USA, 4–8 May 1998; p. OTC-8831.
15. Zhao, Z.; Zhou, M.; Hu, Y.; Hossain, M.S. Behavior of soil heave inside stiffened caissons being installed in clay. *Can. Geotech. J.* **2018**, *55*, 698–709. [CrossRef]
16. Han, C.; Chen, X.; Liu, J. Physical and numerical modeling of dynamic penetration of ship anchor in clay. *J. Waterw. Port Coast. Ocean. Eng.* **2019**, *145*, 04018030. [CrossRef]

Disclaimer/Publisher's Note: The statements, opinions and data contained in all publications are solely those of the individual author(s) and contributor(s) and not of MDPI and/or the editor(s). MDPI and/or the editor(s) disclaim responsibility for any injury to people or property resulting from any ideas, methods, instructions or products referred to in the content.